Nuclear Engineering and Design 248 (2012) 72–81

Contents lists available at SciVerse ScienceDirect

Nuclear Engineering and Design

journal homepage: www.elsevier.com/locate/nucengdes

Verification and Validation of a thermal stratification experiment CFD simulation

Hugo C. Rezende[a,b,*], André A.C. Santos[b,c], Moysés A. Navarro[b], Elizabete Jordão[a]

[a] Faculdade de Engenharia Química, Universidade Estadual de Campinas – UNICAMP, Av. Albert Einstein, 500, 13.083-852 Campinas, SP, Brazil
[b] Centro de Desenvolvimento da Tecnologia Nuclear, Comissão Nacional de Energia Nuclear, Av. Pres. Antônio Carlos, 6627 – 30270-901 Belo Horizonte, MG, Brazil
[c] Departamento de Engenharia Mecânica, Universidade Federal de Minas Gerais, Av. Pres. Antônio Carlos, 6627 – 30270-901 Belo Horizonte, MG, Brazil

ARTICLE INFO

Article history:
Received 2 December 2011
Received in revised form 9 March 2012
Accepted 21 March 2012

ABSTRACT

Thermal stratification and striping are observed in many piping systems including those of nuclear power plants. Periodic occurrences of these thermal transients lead to fatigue and may induce undesirable failures and deformations to the piping. The Thermal Hydraulic Laboratory of the Centro de Desenvolvimento da Tecnologia Nuclear/Comissão Nacional de Energia Nuclear (CDTN/CNEN) conducts an experimental and numerical project simulating the thermal stratified flows in piping systems of pressurized water reactors (PWR) to obtain some understanding on these phenomena. Experiments were carried out in a test section simulating the steam generator injection nozzle of a PWR. A numerical simulation of one experiment was performed with the commercial finite volume Computational Fluid Dynamic code CFX 13.0. A vertical symmetry plane along the pipe was adopted to reduce the geometry in one half, reducing mesh element size and minimizing processing time. The RANS two equations RNG k–ε turbulence model with scalable wall function and the full buoyancy model were used in the simulation. In order to properly evaluate the numerical model it was performed a Verification and Validation (V&V) process. Numerical uncertainties due to mesh refinement and time step were evaluated. This validation process showed the great importance of a proper quantitative evaluation of numerical results. In past studies qualitative evaluations were considered enough and numerical results like the one presented here could be considered satisfactory for the prediction of thermal stratified flows. However, with the present V&V study it was possible to identify objectively the strengths and weaknesses of the model.

1. Introduction

Single-phase thermally stratified flows occur in piping systems where two different layers of the same liquid flow separately without appreciable mixing due to the difference in temperature (and density) and low velocities. This condition results in a varying temperature distribution in the pipe wall and in an excessive differential expansion between the upper and lower parts of the pipe threatening its integrity.

Some safety related piping systems connected to reactor coolant systems in operating nuclear power plants are known to be potentially susceptible to fatigue resulting from thermally stratified flows. Piping systems of PWR plants typically related with thermal stratification are pressurizer surge lines, emergency core cooling lines, residual heat removal lines as well as some segments of the main piping system of the primary and secondary cooling loops, such as the hot and cold legs in the primary and the steam generator feedwater piping system in the secondary piping circuits (Häfner, 1990; Schuler and Herter, 2004). Temperature differences of about 200 K can be found in a narrow band around the hot and cold water interface. To assess potential piping system damage due to thermal stratification, it is necessary to determine the transient temperature distributions in the pipe wall. Aiming to improve the knowledge on thermally stratified flow and increase safety in PWR nuclear reactors, several experimental and theoretical investigations have been conducted in the past years (Häfner, 1990; Navarro et al., 2008b). In recent theoretical evaluations, CFD (Computational Fluid Dynamic) analysis using three dimensional Reynolds Averaged Navier Stokes (RANS) has been used and evaluated (Farkas and Tóth, 2010; Walker et al., 2010; Navarro et al., 2008a,b).

However, before CFD can be considered as a reliable tool for the analysis of thermal stratification there is a need to establish the credibility of the numerical results. Procedures must be defined to evaluate the error and uncertainty due to aspects such as mesh refinement, time step, turbulence model, wall treatment and appropriate definition of boundary conditions. These procedures

* Corresponding author at: Centro de Desenvolvimento da Tecnologia Nuclear, Comissão Nacional de Energia Nuclear, Av. Pres. Antônio Carlos, 6627 – 30270-901 Belo Horizonte, MG, Brazil. Tel.: +55 31 3069 3124; fax: +55 31 3069 3411.
E-mail address: hcr@cdtn.br (H.C. Rezende).

0029-5493/$ – see front matter © 2012 Elsevier B.V. All rights reserved.
http://dx.doi.org/10.1016/j.nucengdes.2012.03.044

are referred to as Verification and Validation (V&V) processes (Roache, 2009). Some of the most important nuclear organizations of the world have already published reports intended to act as guides on how to address CFD V&V (Mahaffy et al., 2007; IAEA, 2003). In 2009 a standard was published by the American Society of Mechanical Engineers (ASME) establishing detailed procedures for V&V of CFD simulations (ASME, 2009).

According to this standard the objective of validation is to estimate the modeling error within an uncertainty range. This is accomplished by comparing the result of a simulation (S) and an experiment (D) at a particular validation point. The discrepancy between these two values, called comparison error (E), can be defined by Eq. (1) as the combination of the errors of the simulation ($\delta_S = S - \text{True Value}$) and experiment ($\delta_{exp} = D - \text{True Value}$) to an unknown True Value.

$$E = S - D = \delta_S - \delta_{exp} \quad (1)$$

The simulation error can be decomposed in input error (δ_{input}) that is due to geometrical and physical parameters, numerical error (δ_{num}) that is due to the numerical solution of the equations and modeling error (δ_{model}) that is due to assumptions and approximations. Splitting the simulation error in its three components and expanding Eq. (1) to isolate the modeling error, it gives Eq. (2).

$$\delta_{model} = E - (\delta_{inum} + \delta_{input} - \delta_{exp}) \quad (2)$$

Then, the standard applies to this analysis the same concepts of error and uncertainty used in experimental data analysis, defining a validation standard uncertainty, u_{val}, as an estimate of the standard deviation of the parent population of the combination of the errors in brackets in Eq. (2), in such a way that the modeling error falls within the range $[E + u_{val}, E - u_{val}]$, or using a more common notation:

$$\delta_{model} = E \pm u_{val} \quad (3)$$

Supposing that the errors are independent, u_{val} can be defined as Eq. (4).

$$u_{val} = \sqrt{u_{num}^2 + u_{input}^2 + u_{exp}^2} \quad (4)$$

The estimation of these uncertainties is at the core of the process of validation. The experimental uncertainty can be estimated by well established techniques (ISO, 1993). Input uncertainty is usually determined by propagation techniques (ASME, 2009) or analytically. The numerical uncertainty, on the other hand, poses greater difficulties to assess.

The estimation of the numerical uncertainty is called verification and is usually split into two categories: code and solution verification. Code verification evaluates the mathematical correctness of the code and is accomplished by simulating a problem that has an exact solution and verifying if that solution were obtained. This activity requires extensive programming access to the core of the code which is not available in commercial codes and is expected to be performed and documented by the supplier (ASME, 2009).

Solution verification is the process of estimating the numerical uncertainty for a particular solution of a problem of interest. The two main sources of errors here are the discretization and iteration processes. The discretization error is the difference between the result of a simulation using a finite grid in time and space and that obtained with an infinitely refined one. The methods developed to evaluate it are based on a systematic grid refinement study where the solution is expected to asymptotically approximate the exact value as the grid is refined, at a rate proportional to the discretization order of the solution. The iteration error is present in codes that use iterative solvers, where the result must converge to the exact value as the iterations develop. It is usually estimated using the residual root mean square (RMS) between subsequent iterations of a variable over all the volumes of the domain (ANSYS, 2010).

Table 1
Boundary conditions for the experiment and simulations.

	Flow rate (kg/s)	P_{gauge} (bar)	T_{hot} (°C)	T_{cold} (°C)
CFX and experiment	0.76	21.1	219.2	31.7
δ[a]	0.03	0.5	2.4	2.4

[a] Global uncertainty.

This paper summarizes a numerical methodology used for the simulation of single-phase thermally stratified flow experiments performed in a pipe similar to the steam generator nozzle of a nuclear reactor at CDTN/CNEN Thermal Hydraulic Laboratory. A V&V evaluation of the numerical model according to the ASME (2009) standard was performed.

2. Experimental methodology

Fig. 1 shows a diagram of the experimental facility. A vessel simulates the steam generator tank and a stainless steel piping system ($D = 0.1223$ m) with a vertical to horizontal curve simulates the steam generator injection nozzle. Both vessel and piping system were insulated using 2 in. thick stone wool covered with aluminum sheets to minimize thermal loss to the ambient. In a typical test, both the vessel and the piping system are initially filled with cold water which is then heated and pressurized by injecting steam from a boiler. As the foreseen pressure and temperature are reached, the water is circulated in the pipe (gray painted region in Fig. 1) to promote its temperature homogenization. After this previous conditioning, the experiment begins with the injection of cold water at low flow rate at the bottom end of the vertical pipe segment. The water leaves the piping system through eleven upper holes at the horizontal segment of the pipe inside the vessel.

Wall and fluid temperatures are measured with type K thermocouples 0.5 mm in diameter, distributed in three measuring stations (1–3). In each measuring station fluid thermocouples are positioned along the tube vertical diameter and along the inner wall perimeter, 3 mm away from the wall. Thermocouples were also brazed along the outer wall perimeter. Two thermocouples installed at position "A" aim to synchronize the experimental and numerical cold water front arrival. The inlet cold water temperature is also measured with type K thermocouples. The measurement of the injected water flow rate is obtained by means of a set of orifice plate and differential pressure transducer and the system pressure by a gauge pressure transducer.

The driving parameter considered to characterize flow under stratified regime due to difference in specific masses is the Froude Number. Different Froude Numbers, from 0.018 to 0.43, were obtained in different testes by setting injection cold water flow rates and hot water initial temperatures. This Froude Number range corresponds to that found in the steam generator injection nozzle during the plant start up.

3. Numerical methodology

The numerical simulation of an experiment with Froude Number 0.146 was performed in a simplified geometry by using CFX 13.0 (ANSYS, 2010) code. Others parameters of the experiment are shown in Table 1. The geometry in Fig. 1 was simulated with the omission of the flanges and most of the lower inlet geometry, as shown in Fig. 2. A previous study (Navarro et al., 2008b) showed that these simplifications have no significant influence on the results.

The computational model was generated with two domains: one solid, corresponding to the pipes walls, and one fluid for the

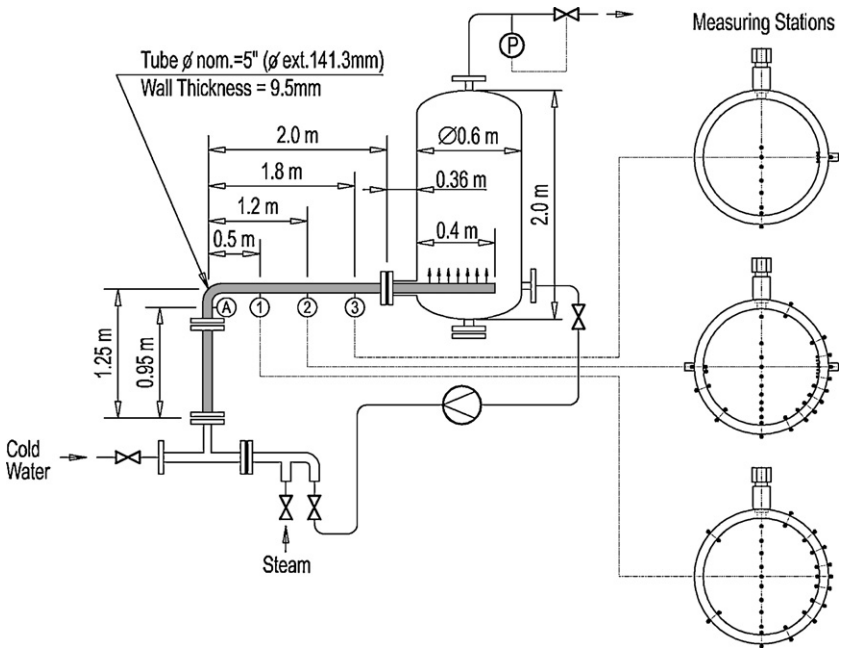

Fig. 1. Diagram of the experimental facility test section and thermocouple distribution at measuring stations 1–3.

water in its interior. A vertical symmetry plane along the pipe was adopted to reduce the mesh size in one half, minimizing processing time. Although the entrance pipe and the elbow curve can cause cross-flow and non-symmetric flow, previous study showed that the thermally stratified flow thermal profile is symmetric in the horizontal (Navarro et al., 2008c). The external tube walls and the internal vessel walls were considered adiabatic. Mass flow inlet and outlet conditions were defined, respectively, at the lower end of the pipe and at the upper end of the vessel. Fig. 2 shows the computational model's details.

The initial conditions shown in Table 1 were used in the simulations. Water properties like density, viscosity and thermal expansion coefficient were adjusted by regression as function of temperature with data extracted from Table IAPWS-IF97 (Wagner and Pruβ, 2002), in the simulation range (25–221 °C).

The RANS – Reynolds Averaging Navier–Stokes equations, the two equations of the RNG k–ε turbulence model, with scalable wall functions, the full buoyancy model and the total energy heat transfer model with the viscous work term were solved. Terms to account for the production and dissipation of turbulence due to buoyancy effects were included in the turbulence model. Although the RNG k–ε turbulence model may not be theoretically the most recommended model for thermal stratification modeling, our experience is that it is a simpler model with stable convergence behavior and smaller running time, which makes it a good candidate for more practical applications in analysis and development of industrial geometries.

The simulations were performed using parallel processing with up to six workstations with two 4 core processor and 24 GB of RAM. All simulations were performed using the high resolution numerical scheme (formally second order) for the discretization of the conservation and RNG k–ε turbulence model equations terms and second order backward Euler scheme for the transient terms. A root mean square (RMS) residual target value of 10^{-6} was defined as the convergence criteria for the simulations in double precision. By using this RMS target the interactive error is minimized and can be neglected in the uncertainty evaluation as its contribution are usually many orders lower than the ones from other sources such as discretization (Roache, 2009).

A mesh and time step study described in the following section was performed according to ASME V&V 20 (ASME, 2009) standard to assess the numerical uncertainty. After this process the verified numerical results were compared with the experimental results in a validation process, also according to V&V ASME standard.

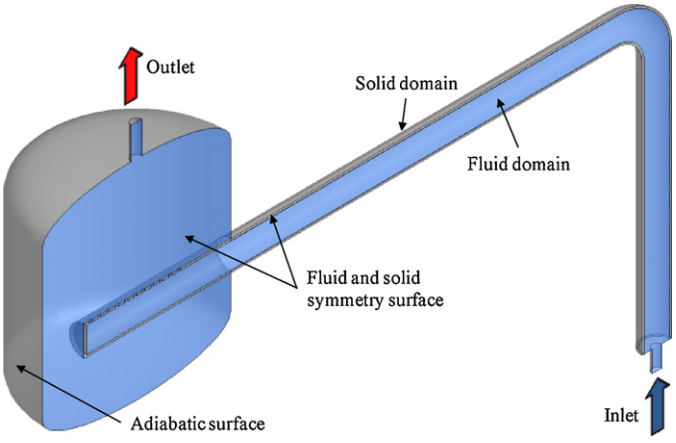

Fig. 2. Computational model domains and boundary conditions.

3.1. Discretization investigation

A solution verification study was performed according to ASME CFD Verification and Validation standard (ASME, 2009) to evaluate mesh and time step uncertainties. Three gradually refined non-structured tetrahedral meshes with prismatic near wall elements (inflated) were generated for the model presented in Fig. 2 to evaluate mesh related uncertainty. Progressive grid refinements were applied to edge sizing of the piping system elements. The ratio between the height of the last prismatic layer and the first tetrahedral was kept equal to 0.5 for all meshes. Three layers of prismatic structured volumes were built close to the surfaces in the solid and fluid domains to capture boundary layer effects and yielded an average y^+ equal to 5, 10 and 20 for meshes 1 (most refined), 2 and 3, respectively. The growth factor between prismatic layers

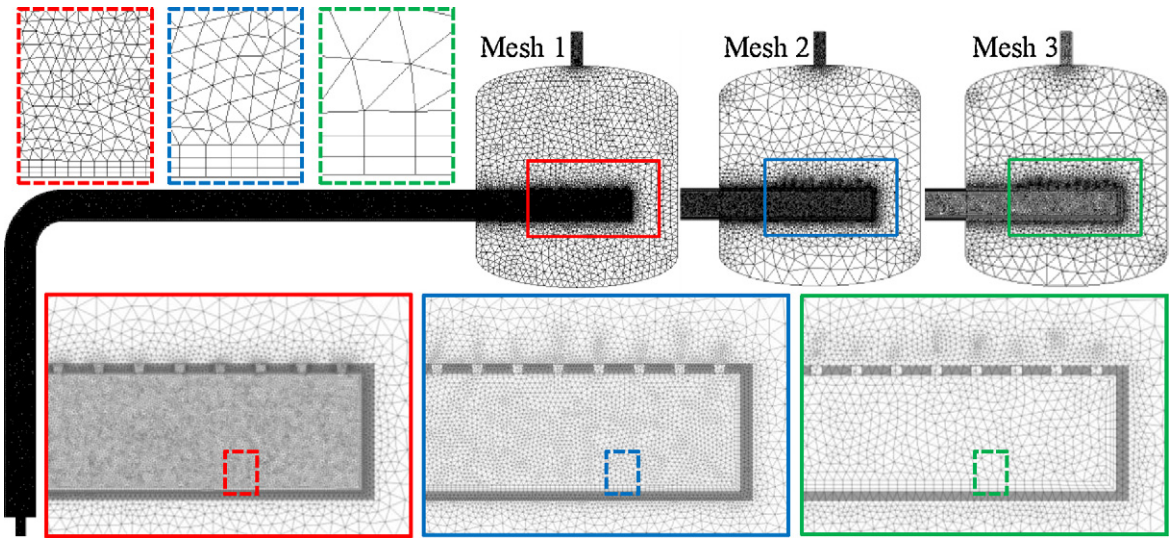

Fig. 3. Mesh details.

Table 2
Meshes characteristics.

Mesh, i	h_i (mm)	No. of elements/nodes	r_i	Element edge length (mm)
1	2.84	2,809,114/13,533,642	1.83	2.5
2	5.22	583,012/2,191,174	1.67	5.0
3	8.70	198,152/472,909	–	10.0

Table 3
Time steps characteristics.

Time, j	t_j (s)	r_j
1	0.075	1.51
2	0.113	1.50
3	0.169	–

was maintained constant with a recommended value of 1.2 (ANSYS, 2010). A localized mesh edge sizing of 5 mm was applied at the inlet nozzle of the vertical pipe and vessel outlet nozzle for all meshes. At the outlet holes of the horizontal pipe an edge sizing of 2 mm was also used for all meshes. Element sizing in the vessel was set to expand freely with a growth factor of 1.2.

Fig. 3 shows some details of the generated meshes. The characteristics of the generate meshes are shown in Table 2. The table includes the resulting grid refinement ratio (r_i) and representative grid edge size (h_i) defined by Eqs. (5) and (6), respectively.

$$r_i = \frac{h_{\text{last coarse mesh}\ \ i+1}}{h_{\text{present mesh}\ \ i}} \tag{5}$$

$$h_i = \left(\frac{\text{Model volume}}{\text{Number of elements of mesh}\ \ i}\right)^{1/3} \tag{6}$$

To evaluate time step related uncertainty, three gradually refined time steps shown in Table 3 were used for the simulation of the model with mesh 2 presented in Fig. 3. Table 3 includes the resulting time step refinement ratio (r_j) defined by Eq. (7).

$$r_j = \frac{t_{\text{last coarse time step}\ \ j+1}}{h_{\text{present time step}\ \ j}} \tag{7}$$

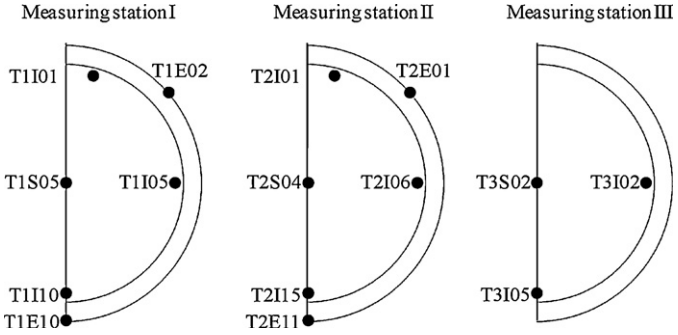

Fig. 4. Thermocouples positions.

4. Results

4.1. Solution verification

Solution verification was performed using the three generated meshes and three simulated time steps based on the Grid Convergence Index method (GCI) of the ASME V&V 20 standard (ASME, 2009). The theoretical basis of the method is to assume that the results are asymptotically converging towards the exact solution of the equation system as the discretization is refined with an apparent order of convergence (p) that is in theory proportional to the order of the discretization scheme. The objective of the method is to determine a 95% confidence interval ($\pm u_{\text{num }95\%} = \pm\text{GCI}$) containing the exact solution, by utilizing three systematically refined discretizations. In other word, the objective is to determine the expanded uncertainty interval due to the discretization.

Considering the representative grid edge sizes $h_{i-1} < h_i < h_{i+1}$ and grid refinement ratios $r_i = h_{i+1}/h_i$, the apparent order of convergence p can be determined by Eqs. (8)–(10) (Celik et al., 2008). In an analogous manner similar equations can be obtained for time discretization. However, it will be omitted for brevity.

$$p_i = \frac{1}{\ln(r_i)}\left|\ln\left|\frac{e_{i+1}}{e_i}\right| + q(p_i)\right| \tag{8}$$

$$q(p_i) = \ln\left(\frac{r_i^{p_i} - s}{r_{i+1}^{p_i} - s}\right) \tag{9}$$

Table 4
Verification process results for several thermocouple positions.

Position in the pipe	Mesh			Time step		
	p_m [a]	GCI_m [a] (°C)	Maximum GCI_m (°C)	p_t [a]	GCI_t [a] (°C)	Maximum GCI_t (°C)
Internal						
T1I01	1.58	14.012	41.608	1.00	0.056	0.173
T1I05	1.88	1.174	35.020	1.32	0.415	17.257
T1I10	1.52	0.496	75.830	1.27	0.578	45.339
T2I01	1.32	7.394	22.829	1.31	0.030	0.218
T2I06	1.87	1.377	51.166	1.22	0.594	21.577
T2I15	1.48	1.489	99.554	1.20	0.748	70.006
T3I02	1.80	1.099	64.103	1.21	0.544	13.988
T3I05	1.47	1.220	122.122	1.23	0.584	51.247
Probe						
T1S05	1.64	2.034	60.014	1.23	0.546	14.964
T2S04	1.65	1.766	58.885	1.16	0.902	15.776
T3S02	1.44	2.381	45.358	1.32	0.796	20.076
External						
T1E02	1.61	2.198	6.347	1.05	0.010	0.095
T1E10	1.56	0.199	0.601	1.21	0.087	0.537
T2E01	1.34	0.164	1.115	1.17	0.003	0.015
T2E11	1.16	1.599	3.302	1.47	0.0185	0.621

[a] Time averaged values.

$$s = 1 \cdot sgn\left(\frac{\varepsilon_{i+1}}{\varepsilon_i}\right) \tag{10}$$

where $\varepsilon_{i+1} = \phi_{i+2} - \phi_{i+1}$, $\varepsilon_i = \phi_{i+1} - \phi_i$, ϕ_k denotes the variable solution on the kth grid and sgn is the signal function ($\mathrm{sgn}(x) = -1$ for $x < 0$; 0 for $x = 0$ and 1 for $x > 0$).

It is recommended that the obtained value of p be limited to the maximum theoretical value, which for the used high resolution and Euler discretization scheme is 2 (ASME, 2009). Also the value of p can be limited to a minimum of 1 to avoid exaggerations of the predicted uncertainty. However, it is recommended that the obtained value be presented for comparison, when it is limited.

With the value of p the expanded uncertainty GCI can be calculated using Eq. (11) using an empirical Factor of Safety, Fs, equal to 1.25, which is the recommended value by the standard for solution verification studies using three or more meshes (ASME, 2009).

$$GCI_i = \frac{Fs \cdot \varepsilon_i}{r_i^{p_i} - 1} \tag{11}$$

When the presented procedure is applied to obtain the GCI for local variables, such as a temperature profile, an average value of p should be used to represent a global order of accuracy (Celik et al., 2008).

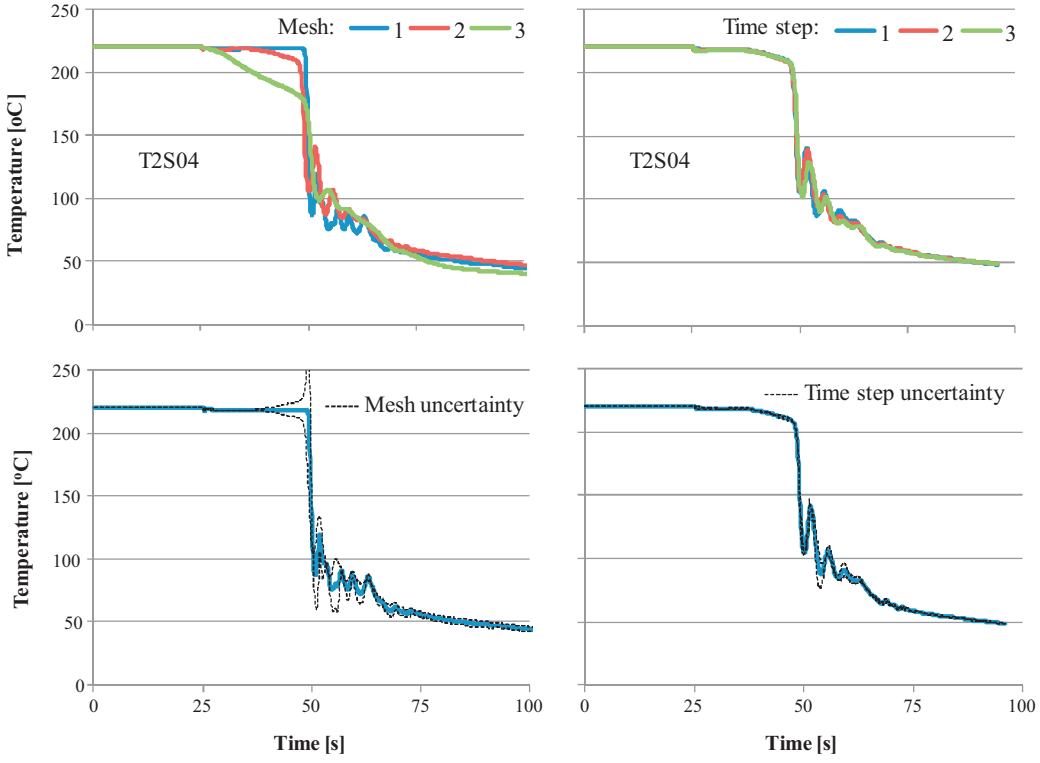

Fig. 5. Numerical uncertainty evaluation due to the mesh and time step.

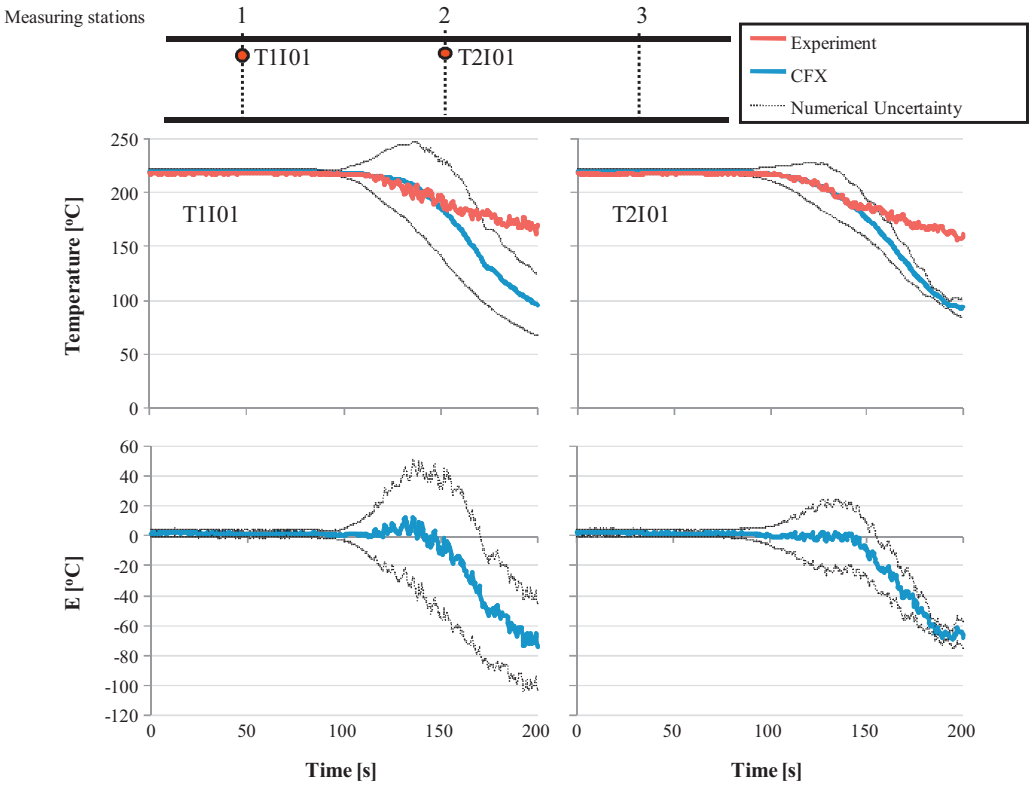

Fig. 6. Validation for the upper thermocouples.

Mesh and time step uncertainties are considered independent in this study and the total numerical expanded uncertainty is calculated through Eq. (12).

$$U_{num} = \sqrt{GCI^2_{mesh} + GCI^2_{time\ step}} \quad (12)$$

In this study the temperature profiles along time were evaluated in several positions of the test section. Fig. 4 displays the analyzed positions that are equivalent to the thermocouple positions of the experiments.

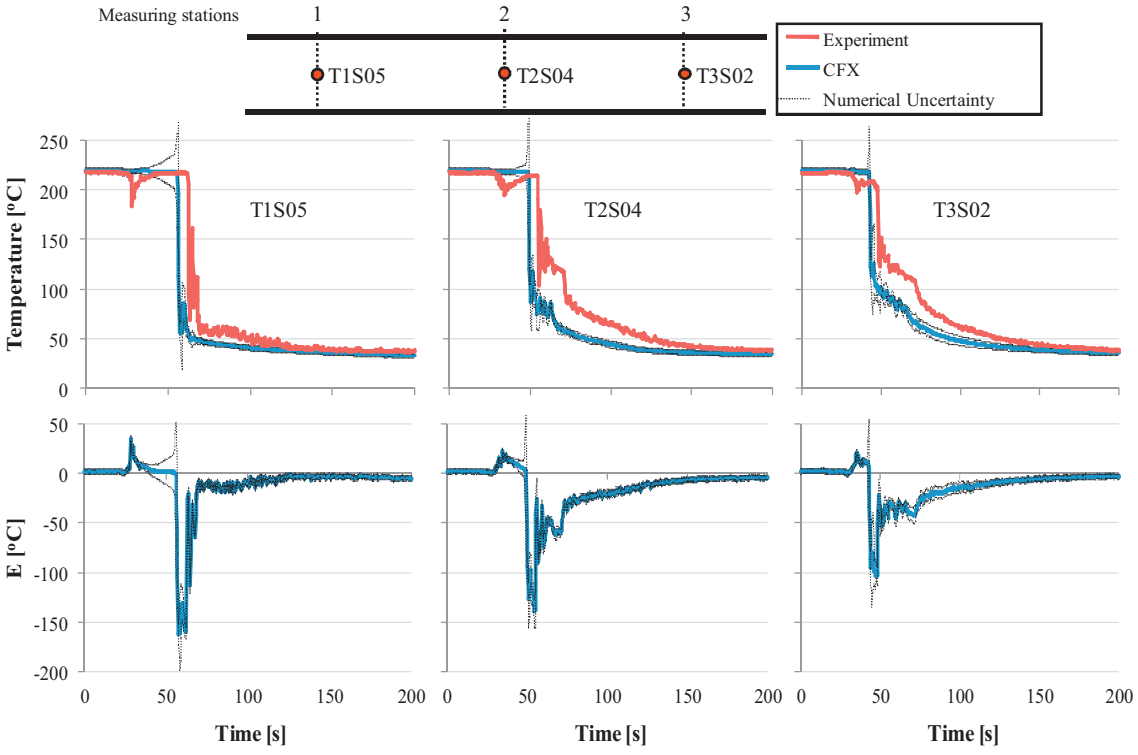

Fig. 7. Validation results for the probe thermocouples.

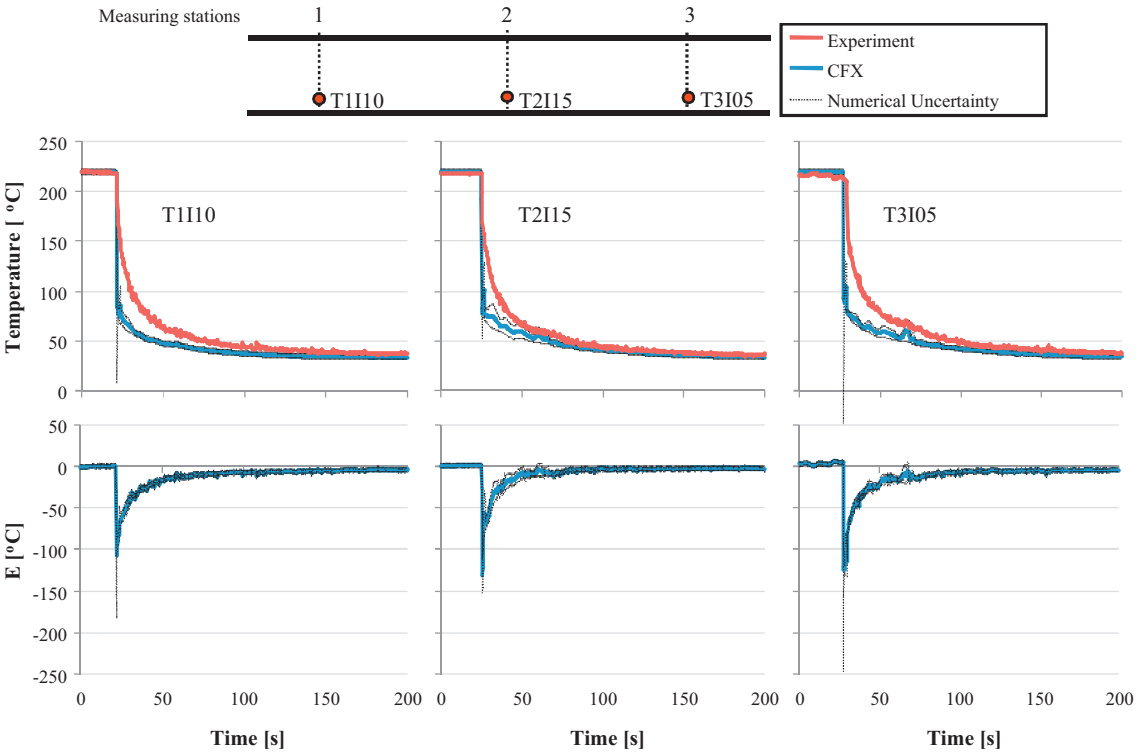

Fig. 8. Validation results for the lower thermocouples.

Table 4 shows the obtained results of the performed verification process. Average values for p and GCI are presented as the maximum GCI of the entire profile. These maximums were all located in regions of steep temperature gradients, which explain the very high values observed.

It can be observed in Table 4 that uncertainties due to the mesh are in average greater than those due to the time step. One reason for these values could be attributed to the least refined mesh used in the study, Mesh 3 shown in Table 2. This mesh could be too coarse and as the uncertainty estimation relies on three meshes this could

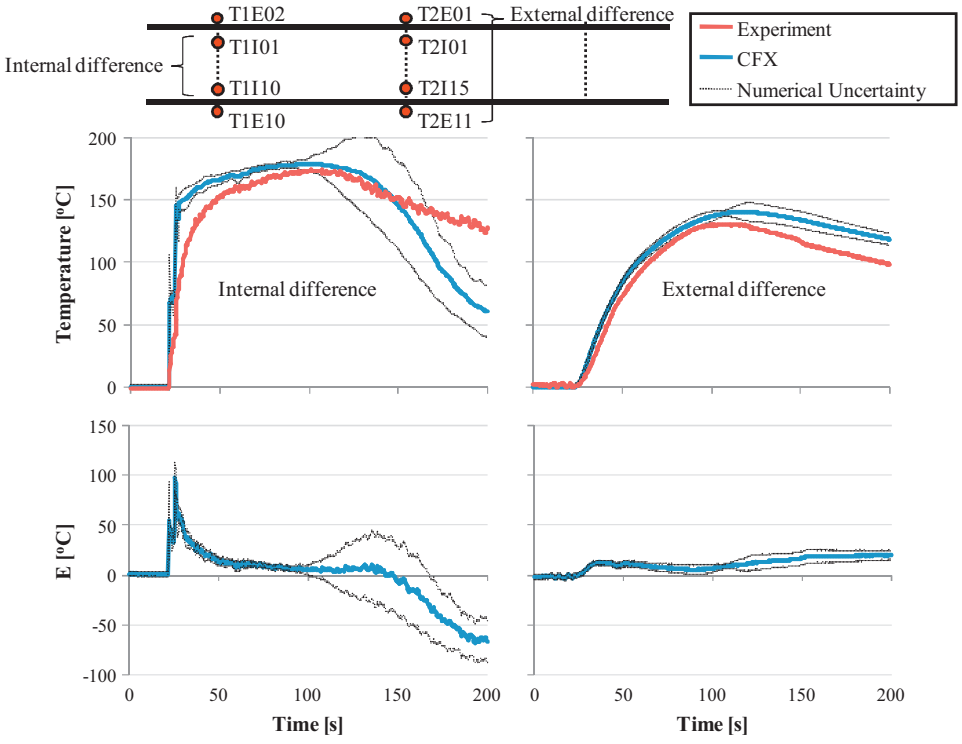

Fig. 9. Validation results for the temperature difference between upper and lower thermocouples positioned internally and externally.

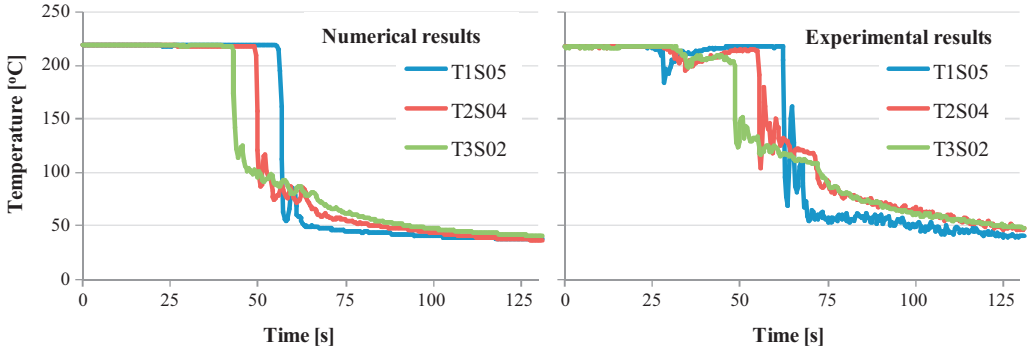

Fig. 10. Numerical and experimental results for the probe thermocouples.

lead to an overestimation of the total uncertainty for the refined mesh. Only thermocouples T1I01 and T2I01 displayed numerical average uncertainties greater than the experimental one (2.4 °C). Both thermocouples are located in the upper region of the vertical tube which indicates that this region is the most affected by the mesh refinement.

An example of the obtained results from the verification process is shown in Fig. 5 that displays the temperature profiles along the time at thermocouple position T2S04 obtained by the simulated meshes and time steps and the associated uncertainties. It is observed that the mesh contribution to uncertainty is much greater than that of the time step. The higher values of uncertainty were obtained at the abrupt temperature drop region and at the subsequent temperature oscillation period.

4.2. Validation

Following the solution verification, a validation process was performed comparing the numerical results with experimental data. The presented numerical results were obtained with the finest mesh and time step studied. To determine the validation expanded uncertainty, u_{val} (Eq. (4)), only the estimated numerical and experimental uncertainties were considered. The input contribution was neglected. Although the input uncertainty is in fact non-neglectable, its evaluation is beyond the purpose of this study as it is extremely complex and requires hundreds of simulations taking in account fabrication tolerances and uncertainties in all measurable variables.

Fig. 6 shows a comparison between numerical and experimental results as well as the validation error ($E = S - D$) and validation uncertainty for the upper thermocouples. Very high validation uncertainty after the beginning of the temperature drop can be observed. This high uncertainty is attributed to the mesh that influences greatly the results in this region. Validations become poor after 150 s of simulation. Before that time, however, the numerical and experimental results present a good agreement.

Figs. 7 and 8 show a comparison between numerical and experimental results with the validation uncertainty and the validation error ($E = S - D$), respectively, for the probe and lower thermocouples. Results for both regions show a high validation error and uncertainty for the beginning of the temperature drop and subsequent oscillations. It is observed that the cold water front reaches the center of the pipe (probe thermocouples) before the experiment and that the temperature drop in the lower region of the pipe is quicker in the simulation. Although considerable validation error is observed, the qualitative agreement between experiment and simulation can be considered good as most of the behavior observed was reproduced.

Fig. 9 shows the evolution of the temperature differences between the average temperatures on the highest and lowest positions of the horizontal tube calculated through Eq. (13) for the internal and external thermocouples.

$$DT = \frac{(T_1^u + T_2^u) - (T_1^l + T_2^l)}{2} \tag{13}$$

where the superscripts u and l are relative, respectively, to the upper and the lower positions and subscripts 1 and 2, respectively, to measuring stations 1 and 2 of the horizontal tube.

As can be seen from Fig. 9, for the region of highest temperature difference, which is most critical for the piping system integrity, the validation error is relatively low and well predicted. It is also observed that the external temperature difference presents good agreement between experimental and numerical results during the evaluated time.

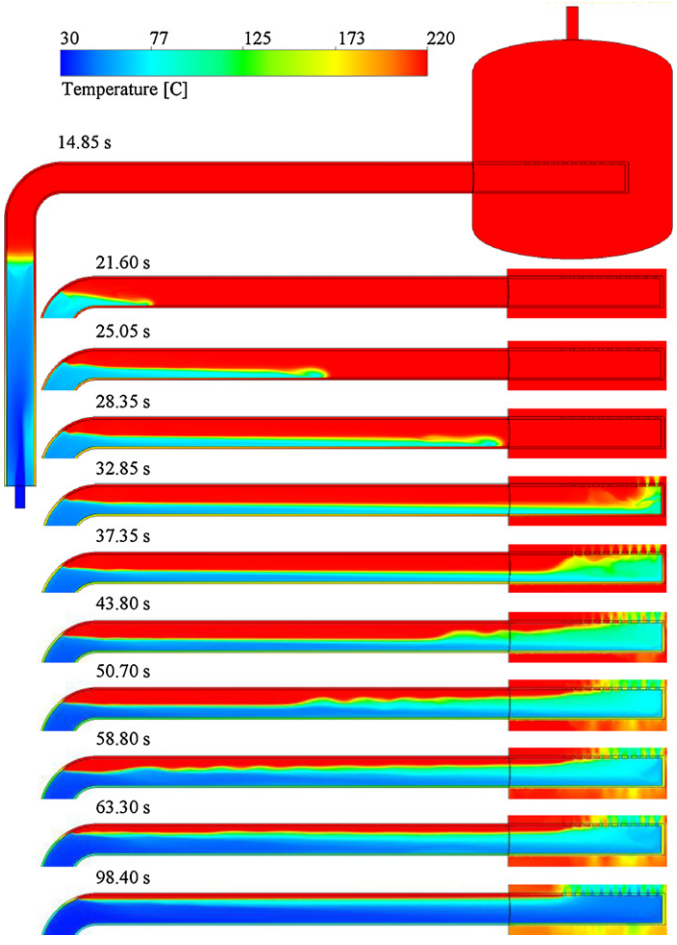

Fig. 11. Temperature contours evolution along time.

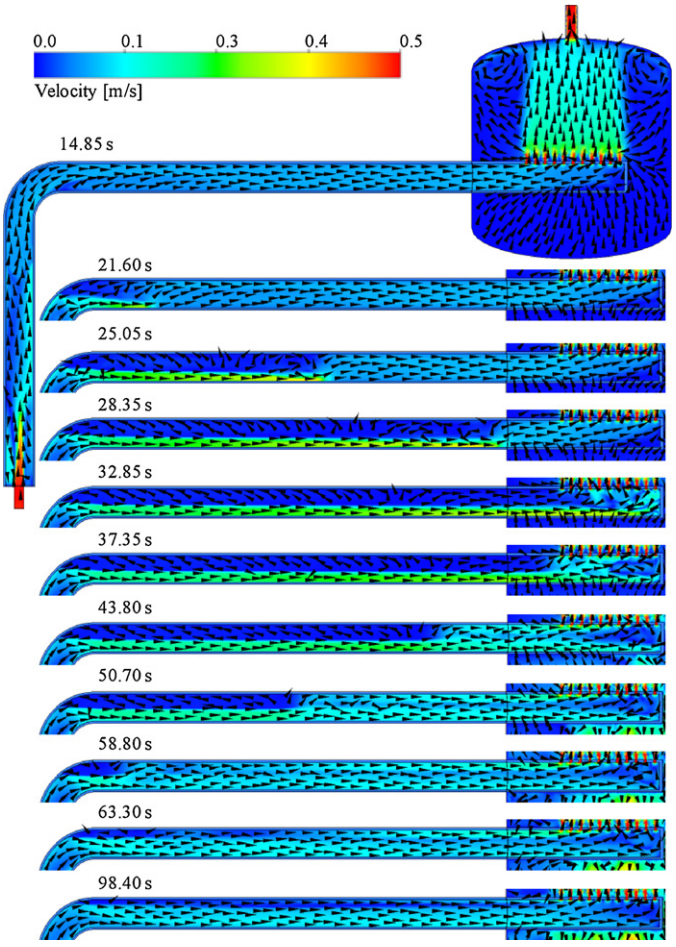

Fig. 12. Flow velocity behavior along time.

It can be observed that the numerical model reproduced the general flow behavior of the experiments by a qualitative standpoint. Fig. 10 shows the numerical and experimental temperature evolutions at middle high thermocouple positions at the three measuring stations. The experimental results show an early and temporary cooling that occurred successively at thermocouples T1S05, T2S04 and T3S02, followed by a sudden and permanent cooling that occurred successively in thermocouples T3S02, T2S04 and T1S05. The early cooling was not observed in the numerical simulation but the sudden and permanent cooling was reproduced in the same sequence, in a direction opposite to the cooling of the lower thermocouples shown in Fig. 8. Both numerical and experimental results also show that the thermocouples were cooled to different temperature levels with T1S05 being the coolest one.

These results indicate that the cold water front hits the wall at the end of the horizontal pipe and the cold water starts filling the pipe in the opposite direction from the end wall to the curve as a second cold water front, while the hot water re-circulates at the top of the pipe. This could be observed numerically in Fig. 11 that shows the cold water front evolution along time.

It can also be observed in Fig. 11 that a cold water "head" is formed as the cold water front advances in the horizontal pipe. Even though in the numerical solution this "head" was not high enough to influence the temperature of the water at the middle of the pipe, this flow structure could explain the temperature reduction and rise observed experimentally between 25 and 50 s. This phenomenon occurred for all thermocouples as shown in Fig. 10.

Fig. 12 shows details of the flow behavior and flow velocity evolution in the numerical simulation and highlights the previously observed behavior, i.e., as the cold front reaches the end of the pipe it starts filling the pipe in the opposite direction eliminating almost all of the recirculating hot water. However, some hot water remains imprisoned at the top of the pipe as the injected cold water takes control of all water exits holes. This phenomenon is observed experimentally and causes the thermal stratification at the top of the pipe to persist for many minutes.

5. Conclusions

Single-phase thermal stratification was simulated numerically using CFX 13.0 (ANSYS, 2010) and experimentally in a piping system similar to the steam generator injection nozzle at the secondary loop of a pressurized water reactor (PWR). The experimental and numerical simulations were carried out with a mass flow rate of 0.76 kg/s, corresponding to a Froude Number of 0.146.

A V&V evaluation of the numerical CFD methodology based on ASMEs standard (ASME, 2009) was performed. Solution verification was performed using three progressively refined meshes and time steps. Temperature profiles in several positions inside and outside the piping system were evaluated. In average the uncertainties due to the mesh were greater than those due to the time step. One reason for these values could be attributed to the coarse mesh used in the study that could lead to overestimation of the total uncertainty of the refined mesh. Only thermocouples located in the upper region of the vertical tube displayed average uncertainties above the experimental one of 2.4 K, which indicates that this region is the most affected by the mesh refinement.

A validation process was performed according to the ASME V&V 20 standard (ASME, 2009). Very high validation uncertainty after the beginning of the temperature drop could be observed for the thermocouples in the highest positions inside the piping system. This high uncertainty was attributed to the mesh that influences greatly the results in this region. Results for the intermediary and lower regions of the pipe showed a high validation error and uncertainty for the beginning of the temperature drop and during the subsequent oscillations. It was observed that in the numerical simulation the cold water front reaches the center of the pipe before the experiment and that the temperature drop in the lower region of the pipe is quicker in the simulation. This could be associated to model deficiencies as boundary conditions or/and turbulence model. The use of more sophisticated Reynolds stress turbulence models or even LES modeling should be evaluated in the future.

Although considerable validation error was observed the qualitative agreement between experiment and simulation can be considered good as most of the behavior observed was reproduced. The region of highest temperature difference, which is the most critical for the piping system integrity, showed a relatively low validation error and was well predicted. It was also observed that the external temperature difference agreement between experimental and numerical results presented a good agreement during the evaluated time.

The performed validation process showed the importance of proper quantitative evaluation of numerical results. In past studies a qualitative evaluation of the results would be considered sufficient and the present model would be considered satisfactory for thermal stratification prediction and study. However, with the present V&V study it was possible to identify objectively the strengths and weaknesses of the model.

References

ANSYS, 2010. CFX-13.0 User Manuals, Canonsburg, USA.
ASME, 2009. Standard for Verification and Validation in Computational Fluid Dynamics and Heat Transfer – V&V 20. ASME, NY, USA.

Celik, I.B., Ghia, U., Roache, P.J., Freitas, C.J., Coleman, H., Raad, P.E., 2008. Procedure for estimation and reporting of uncertainty due to discretization in CFD applications. J. Fluids Eng. 130, 078001-1–078001-4.

Farkas, T., Tóth, I., 2010. Fluent analysis of a ROSA cold leg stratification test. Nucl. Eng. Des. 240, 2169–2175.

Häfner, W., 1990. Thermische Schichit-Versuche im Horizontalen Rohr. Kernforschungszentrum Karlsruhe GmbH, Karlsruhe, Germany.

ISO, 1993. Guide to the Expression of Uncertainty in Measurement. ISO, Geneva, Switzerland.

IAEA, 2003. Use of computational fluid dynamics codes for safety analysis of nuclear reactor systems, TECDOC-1379, November, 2003.

Mahaffy, J., Chung, B., Dubois, F., Dubois, F., Graffard, E., Heitsch, M., Henriksson, M., Komen, E., Moretti, F., Morii, T., Mühlbauer, P., Rohde, U., Scheuerer, M., Smith, B.L., Song, C., Watanabe, T., Zigh, G., 2007. Best practice guidelines for the use of CFD in nuclear reactor safety applications. Organisation for Economic Co-operation and Development, Report NEA/CSNI/R(2007)5. http://www.nea.fr/html/nsd/docs/2007/csni-r2007-5.pdf.

Navarro, M.A., Rezende, H.C., Santos, A.A.C., 2008a. Experimental and numerical investigation of thermal stratified flow in horizontal pipes. In: European Thermal-Sciences Conference – EUROTHERM, Eindhoven, Netherlands (paper code MCV-2).

Navarro, M.A., Rezende, H.C., Santos, A.A.C., Pinto, J.P.F., 2008b. Thermal hydraulic analysis of a thermal stratified flow in a horizontal piping. In: 7th International Topical Meeting on Nuclear Reactor Thermal Hydraulics Operation and Safety – NUTHOS-7, Seoul, Korea.

Navarro, M.A., Rezende, H.C., Santos, A.A.C., Carvalho, H., 2008c. Numerical and experimental simulation of the thermal stratification in a horizontal pipe. Int. J. Transp. Phenom. 10, 215–221.

Roache, P.J., 2009. Fundamentals of Verification and Validation. Hermosa Publishers, Socorro, USA.

Schuler, X., Herter, K.H., 2004. Thermal fatigue due to stratification and thermal shock loading of piping. In: 30th MPA – Seminar in Conjunction with the 9th German-Japanese Seminar, Stuttgart, Germany, pp. 6.1–6.14.

Wagner, W., Pruβ, A., 2002. The IAPWS formulation 1995 for the thermodynamic properties of ordinary water substance for general and scientific use. J. Phys. Chem. Ref. Data 31, 387–535.

Walker, C., Manera, A., Niceno, B., Simiano, M., Prasser, H.M., 2010. Steady-state RANS-simulations of the mixing in a T-junction. Nucl. Eng. Des. 240, 2107–2115.